Astron. Astrophys. 322, 19–28 (1997)

ASTRONOMY AND ASTROPHYSICS

A radio continuum survey of Shapley-Ames galaxies at λ 2.8 cm

II. Separation of thermal and non-thermal radio emission

S. Niklas[1,2], **U. Klein**[3], **and R. Wielebinski**[2]

[1] Max-Planck-Institut für Kernphysik, Postfach 10 39 80, D-69029 Heidelberg, Germany
[2] Max-Planck-Institut für Radioastronomie, Auf dem Hügel 69, D-53121 Bonn, Germany
[3] Radioastronomisches Institut, Universität Bonn, Auf dem Hügel 71, D-53121 Bonn, Germany

Received 28 May 1996 / Accepted 5 July 1996

Abstract. The radio continuum spectra of 74 galaxies were used to separate thermal and non-thermal radio emission. The thermal fraction f_{th}^{1GHz} at 1 GHz and the non-thermal spectral index α_{nth} of the radio continuum emission were determined. The mean values are $\langle f_{th}^{1GHz} \rangle = 0.08 \pm 0.01$ and $\langle \alpha_{nth} \rangle = 0.83 \pm 0.02$. Even at 10 GHz the radio continuum emission of most of the galaxies is dominated by the synchrotron component. Using Hα data the thermal radio flux densities were independently estimated and the non-thermal spectral indices were recalculated. Good agreement was found between the results of the two methods and the mean internal extinction was determined to be $A_{H\alpha} \simeq 0.8^m$. Early-type spirals and irregulars tend to have flatter non-thermal spectra as the thermal fraction is independent of morphological type. Galaxies with strong star formation activity are found to have flatter non-thermal spectral indices.

Key words: galaxies: spiral – infrared: galaxies – radio continuum: galaxies – ISM: cosmic rays

1. Introduction

The radio continuum emission of spiral galaxies is a composition of two components: the non-thermal synchrotron emission of relativistic electrons gyrating in the interstellar magnetic field and the thermal free-free emission of electrons in photo-ionized gas surrounding hot stars. Owing to the steep spectrum of the synchrotron emission the thermal emission is expected to become more important in the high-frequency regime. The different spectral behaviour can be used for the separation of the two components, and it is absolutely necessary to get high-quality data in the high-frequency regime.

Send offprint requests to: S.Niklas

The spectral index of the synchrotron radiation α_{nth} ($S_\nu^{nth} \propto \nu^{-\alpha_{nth}}$) is directly connected with the spectral index of the energy distribution of the radiating electrons. If the energy distribution of the cosmic ray electrons is given by $N(E)\,dE = KE^{-\gamma}dE$, the non-thermal spectral index becomes $\alpha = (\gamma - 1)/2$. The typical injection spectrum of the electrons is $\gamma \approx 2.1 \cdots 2.3$ (e.g. Bogdan & Völk 1983; Völk et al. 1988). Energy dependent diffusion and energy losses due to synchroton emission and inverse Compton scattering vary the energy distribution of the electrons (e.g. Pacholczyk 1970). The result is a steepening of the observed radio spectrum at high frequencies. In principle one should be able to decide if the cosmic ray electrons lose all their energy within their host galaxy or if they can escape from it, by analyzing the radio spectrum of a galaxy. This question is still under discussion. Chi & Wolfendale (1990) expect efficient confinement in very luminous and massive galaxies. Observational evidence that particle retention is less efficient in low mass and dwarf galaxies was presented by Klein et al. (1991). A model for the tight radio-FIR correlation developed by Völk (1989) predicts a totally loss-dominated radio spectrum, corresponding to a non-thermal radio spectral index $\alpha_{nth} \sim 1$ in the frequency range of a few GHz. The effect of star formation and the FIR-to-radio ratio on the spectrum of a galaxy was further discussed by Condon et al. (1991).

Previous investigations of the radio spectra of galaxies yielded different results. An analysis of the power-law spectral index of 56 spiral galaxies by Gioia et al. (1982) yielded a narrow distribution of the spectral indices. For a sample of 13 galaxies Klein (1988) separated the thermal and non-thermal emission. His mean value of the non-thermal spectral index is $\langle \alpha_{nth} \rangle = 0.88 \pm 0.08$, and he concluded that the radio emission between 1 and 5 GHz is dominated by the non-thermal component. Duric et al. (1988) analyzed the radio spectra of about 30 galaxies and found strong variations in spectral index and thermal fraction from galaxy to galaxy. This was claimed to indicate that the physical conditions in the interstellar medium vary

Table 1. Results of the separation of thermal and non-thermal radio emission

galaxy	type	f_{th}^{1GHz}	α_{nth}	f_{th}^{10GHz}	χ^2_{min}	N_{df}	code for references
NGC 0157	Sc	<0.05	$0.85 - 0.98$	<0.30	2.66	3	1, 2, 3, 4, 5, 6
NGC 0253	Sc	0.10 ± 0.02	0.77 ± 0.04	0.35	1.11	4	2, 10, 11
NGC 0278	Sb	<0.05	$0.71 - 0.84$	<0.30	3.37	1	1, 2, 4, 6 - 9
NGC 0520	Am	<0.09	$0.63 - 0.77$	<0.29	5.96	1	1, 12, 13, 14
NGC 0660	Sa	0.12 ± 0.02	0.81 ± 0.03	0.42	5.22	4	1, 2, 4, 9, 12, 13, 15, 16
NGC 0891	Sb	$0.01^{+0.03}_{-0.01}$	0.78 ± 0.03	0.05	11.04	5	2, 4, 8, 9, 13, 17, 18, 19
NGC 1055	Sb	$0.02^{+0.03}_{-0.02}$	0.81 ± 0.04	0.16	3.13	1	1, 2, 3, 4, 12, 13, 19
NGC 1068	Sb	0.01 ± 0.01	0.74 ± 0.01	0.04	7.61	5	1, 2, 3, 4, 5, 15, 19
NGC 1084	Sc	0.02 ± 0.02	0.86 ± 0.04	0.11	0.22	2	1, 2, 4, 5, 15
NGC 1309	Sb	<0.08	$0.63 - 0.75$	<0.29	4.81	1	1, 2, 3
NGC 1421	Sc	<0.06	$0.59 - 0.68$	<0.20	11.01	1	1, 2, 3, 4
NGC 1569	Sm	0.08 ± 0.04	0.58 ± 0.03	0.21	10.59	1	4, 9, 13, 15, 19, 20 - 23
NGC 2146	Sb	0.11 ± 0.03	1.11 ± 0.05	0.56	0.97	3	1, 2, 4, 13, 14, 15, 19, 25
NGC 2207	Sc	$0.02^{+0.04}_{-0.02}$	0.97 ± 0.03	0.14	0.59	2	1, 2, 4, 15
NGC 2276	Sc	<0.03	$0.93 - 1.01$	<0.21	6.12	2	2, 4, 16, 22, 26, 27, 28
NGC 2903	Sc	0.15 ± 0.04	1.04 ± 0.06	0.62	4.56	4	2, 4, 5, 8, 9, 12, 13, 15, 18, 19
NGC 2964	Sc	$0.03^{+0.05}_{-0.03}$	0.85 ± 0.08	0.15	1.67	2	6, 8, 9, 12, 13, 19
NGC 3031	Sb	0.05 ± 0.02	0.79 ± 0.03	0.21	3.15	4	2, 4, 9, 19, 29, 30, 31
NGC 3034	Am	<0.01	$0.65 - 0.67$	<0.03	26.37	7	2, 4, 19, 32, 33
NGC 3079	Sc	0.08 ± 0.02	0.82 ± 0.03	0.32	15.57	5	1, 2, 4, 9, 13 - 15, 18, 19
NGC 3166	Sa	0.12 ± 0.08	0.72 ± 0.09	0.36	2.23	1	2, 3, 4
NGC 3227	Sb	<0.05	$0.66 - 0.76$	<0.20	9.00	3	1, 2, 4, 12, 13,
NGC 3310	Sbc	0.04 ± 0.03	0.61 ± 0.03	0.14	31.17	5	2, 4, 8, 9, 13, 15, 18, 19
NGC 3351	SBb	$0.02^{+0.05}_{-0.02}$	0.78 ± 0.07	0.09	3.55	3	1, 2, 4, 12, 13, 19, 34
NGC 3504	Sb	$0.01^{+0.04}_{-0.01}$	0.70 ± 0.05	0.04	7.91	4	2, 4, 8, 9, 12 - 15
NGC 3521	Sb	0.04 ± 0.03	1.12 ± 0.07	0.32	1.16	4	1, 2, 4, 5, 12, 15
NGC 3556	Sc	$0.07^{+0.05}_{-0.04}$	0.73 ± 0.06	0.24	0.69	1	1, 2, 4, 9, 13, 18, 19
NGC 3593	Sa	<0.09	$0.63 - 0.77$	<0.32	6.81	2	1 - 4, 9, 12, 13
NGC 3627	Sb	<0.09	$0.68 - 0.82$	<0.35	10.55	4	1, 2, 4, 12, 13, 15, 19
NGC 3628	Sb	<0.11	$0.68 - 0.88$	<0.44	6.85	4	35
NGC 3675	Sb	0.05 ± 0.04	0.73 ± 0.05	0.18	4.85	1	2, 7, 8, 18, 37
NGC 3810	Sc	0.14 ± 0.04	1.09 ± 0.09	0.63	16.40	3	1, 2, 4, 9, 12, 13
NGC 3893	Sc	<0.09	$0.66 - 0.84$	<0.35	4.81	1	1, 2, 4, 8, 9, 18
NGC 3982	Sbc	<0.22	$0.54 - 0.93$	<0.66	2.80	1	7, 8, 18
NGC 4030	Sb	<0.04	$0.73 - 0.80$	<0.18	9.22	3	1, 2, 3
NGC 4038	Sc	0.14 ± 0.02	0.94 ± 0.05	0.54	4.45	5	1, 2, 4, 15
NGC 4051	Sbc	0.03 ± 0.02	0.92 ± 0.05	0.18	1.57	1	2, 8, 9, 18
NGC 4088	SBc	0.09 ± 0.04	0.80 ± 0.07	0.34	2.24	2	1, 2, 4, 8, 9, 18, 19, 37
NGC 4102	Sb	$0.01^{+0.03}_{-0.01}$	0.71 ± 0.05	0.04	2.06	2	4, 7, 8, 9, 14, 18, 19, 37
NGC 4151	Sab	<0.16	$0.65 - 0.91$	<0.57	5.41	2	1, 2, 4, 8, 9, 18
NGC 4192	Sb	0.04 ± 0.04	0.84 ± 0.06	0.19	0.50	2	2, 3, 4, 12, 13, 38
NGC 4254	Sc	0.05 ± 0.03	0.91 ± 0.05	0.26	3.37	4	1, 2, 4, 9, 12, 13, 15, 19, 39, 40, Urbanik p.c.
NGC 4258	Sb	<0.01	$0.77 - 0.83$	<0.05	13.65	5	1, 2, 4, 8, 9, 13, 18, 19
NGC 4321	Sc	<0.05	$0.77 - 0.89$	<0.25	9.23	2	1, 2, 3, 4, 9, 12, 19, 38, 39
NGC 4388	Sab	<0.04	$0.71 - 0.79$	<0.17	19.90	1	2, 9, 12, 38
NGC 4414	Sc	$0.06^{+0.07}_{-0.05}$	0.81 ± 0.09	0.25	1.26	3	2, 4, 6, 8, 9, 12, 14, 18, 37
NGC 4438	Sb	<0.15	$0.59 - 0.64$	<0.39	8.68	1	2, 4, 9, 12, 38
NGC 4449	Sm	0.18 ± 0.02	0.93 ± 0.03	0.59	7.22	3	1, 2, 4, 9, 13, 14, 23
NGC 4490	Scd	0.04 ± 0.02	0.76 ± 0.03	0.16	8.89	5	1, 2, 4, 7, 13, 14, 18, 25
NGC 4501	Sbc	0.09 ± 0.01	1.19 ± 0.04	0.56	3.27	3	1, 2, 4, 9, 12, 38, 39

strongly among the galaxies. Hence, it remains unclear whether the non-thermal radio spectrum and the thermal amount are fixed within the variety of galaxies or if there are large variations of these quantities. The main problem with previous analyses of the radio spectra has been the lack of high-quality radio data at high frequencies. With the Shapley-Ames survey carried out at 10.55 GHz with the 100-m radio telescope of the MPIfR Bonn such a data base at high frequencies has now been established. The observational methods, the data reduction and the results are described by Niklas et al. (1995; Paper I).

In this paper we present the integrated radio spectra of a subsample of the Shapley-Ames sample. In Sect. 2 we present the spectral data and introduce the separation method. Then, in Sect. 3 the results of the separation of the thermal and non-thermal radio emission are given. In Sect. 4 we discuss the question if energy losses of the cosmic-ray electrons have significantly affected the radio spectra. The influence of the properties of the galaxies on the radio spectral indices are investigated in Sect. 5. Finally, we summarize the derived results.

2. Radio spectral data and separation method

We have carried out a literature search in order to collect all integrated radio flux densities of Shapley-Ames galaxies at various wavelengths. All flux densities from the literature were scaled to the calibration scale of Baars et al. (1977). Because of the

Table 1. continued

Galaxie	Typ	f_{th}^{1GHz}	α_{nth}	f_{th}^{10GHz}	χ^2_{min}	N_{df}	code for references
NGC 4527	Sb	0.07 ± 0.03	0.82 ± 0.06	0.29	11.23	1	1 - 4, 12
NGC 4565	Sb	0.11 ± 0.04	1.18 ± 0.11	0.61	1.43	3	40
NGC 4568	Sc	$0.02^{+0.04}_{-0.02}$	0.75 ± 0.07	0.09	5.56	1	1, 2, 12, 38
NGC 4569	Sa	0.07 ± 0.05	0.81 ± 0.08	0.29	0.34	1	2, 12, 38, 39
NGC 4631	Sc	0.03 ± 0.02	0.78 ± 0.04	0.13	4.02	5	2, 4, 8, 9, 12, 13, 18, 19
NGC 4654	Sc	0.17 ± 0.05	0.87 ± 0.06	0.55	8.46	2	2, 12, 34, 38
NGC 4666	Sbc	<0.09	$0.68 - 0.78$	<0.33	13.72	3	1, 2, 4, 41
NGC 4736	Sab	0.18 ± 0.05	0.74 ± 0.06	0.50	1.11	2	1, 2, 4, 8, 9, 13, 18, 19, 25
NGC 4984	Sa	$0.04^{+0.06}_{-0.04}$	0.78 ± 0.08	0.17	1.54	1	2, 3, 14
NGC 5005	Sb	0.09 ± 0.03	1.04 ± 0.05	0.48	1.38	3	1, 2, 4, 8, 9, 15, 18, 19
NGC 5033	Sbc	0.11 ± 0.03	1.03 ± 0.03	0.53	0.81	2	2, 4, 6, 8, 9, 12, 13, 15 ,18, 19
NGC 5054	Sb	<0.08	$0.75 - 0.94$	<0.39	2.88	1	1 - 4
NGC 5055	Sbc	0.09 ± 0.04	0.89 ± 0.06	0.39	5.08	4	1, 4, 6, 8, 13, 15, 19, 37
NGC 5194	Sbc	0.05 ± 0.01	0.94 ± 0.02	0.28	22.20	5	42
NGC 5236	SBc	0.01 ± 0.01	0.85 ± 0.02	0.07	7.91	2	1 - 5, 15, 19, 43
NGC 5248	Sb	0.05 ± 0.03	0.87 ± 0.05	0.28	6.99	4	1 - 3, 12, 13, 15
NGC 5383	SBb	0.12 ± 0.08	0.89 ± 0.16	0.42	0.08	1	44
NGC 5457	Sc	0.05 ± 0.02	0.83 ± 0.03	0.22	6.81	5	1, 2, 4, 8, 18, 19, 4 45
NGC 5676	Sc	$0.01^{+0.03}_{-0.01}$	0.84 ± 0.05	0.05	1.64	1	2, 4, 6, 8, 9, 18
NGC 5792	SBb	$0.01^{+0.03}_{-0.01}$	1.03 ± 0.08	0.10	1.19	1	1, 2, 13, 38
NGC 5907	Sc	0.16 ± 0.04	1.05 ± 0.09	0.63	2.11	3	35
NGC 6946	Sc	0.06 ± 0.01	0.90 ± 0.02	0.13	6.87	4	46
NGC 7331	Sb	<0.06	$0.87 - 1.04$	<0.37	6.08	4	35
NGC 7479	Sb	0.10 ± 0.05	0.79 ± 0.07	0.36	6.00	3	2, 4, 12, 13, 34

code	author	year	code	author	year
1	Haynes et al.	1975	24	Sulentic	1976
2	Condon	1987	25	Klein & Emerson	1982
3	Harnett	1982	26	Hummel & Beck	1995
4	Hummel	1980	27	Urbanik et al.	1985
5	Huchtmeier	1975	28	Branson	1967
6	Duric et al.	1988	29	Segalovitz	1977
7	Gioia & Fabbiano	1987	30	Beck et al.	1985
8	Gioia et al.	1982	31	von Kap-herr et al.	1975
9	Sramek	1975	32	Kellermann et al.	1969
10	Klein et al.	1983	33	Klein et al.	1988
11	Beck et al.	1994	34	Garcia-Baretto et al.	1993
12	Dressel & Condon	1978	35	Dumke et al.	1995
13	Israel & van der Hulst	1983	36	Hummel et al.	1991a
14	Haynes & Sramek	1975	37	Cox et al.	1988
15	Kazés & Nguyen-Quang-Rieu	1970	38	Niklas et al.	1995
16	Wunderlich et al.	1987	39	Urbanik et al.	1986
17	Hummel et al.	1991b	40	Whiteoak	1970
18	Gioia & Gregorini	1980	41	Sukumar et al.	1988
19	Israel & Mahoney	1990	42	Neininger	1992
20	Lequeux	1971	43	Neininger et al.	1991
21	Reakes	1980	44	Gräve et al.	1981
22	Condon	1983	45	Gräve et al.	1990
23	Klein & Gräve	1986	46	Ehle & Beck	1993

increasing amount of the thermal fraction in the high-frequency part of the radio spectrum the data quality of the high-frequency data is important. Hence, we used only those galaxies where the relative flux density error at λ2.8 cm as given in Paper I is below 15 %. In order to increase the statistical significance, all galaxies with flux densities at only three or less frequencies above 400 MHz were eliminated. This lower frequency limit was used to avoid effects of ionization and adiabatic losses of the relativistic electrons. These losses can significantly flatten a radio spectrum in the low-frequency part (e.g. Lerche & Schlickeiser 1982). The remaining sample consists of 74 galaxies.

First of all, a rough estimate of the spectral index was made. Then, using this estimated value, flux densities in narrow frequency bands (e.g. 1400 to 1490 MHz or 10.55 to 10.7 GHz) were scaled to an average frequency. The weighted mean of these scaled flux densities was then computed. The weighting factor was the inverse of the squared flux density error. This turned out to yield more reliable fit results compared to using the individual flux densities at slightly different frequencies. We fitted the following model to the mean integrated radio spectra:

$$\frac{S_\nu}{S_{\nu_0}} = f_{th}^{\nu_0} \left(\frac{\nu}{\nu_0}\right)^{-0.1} + (1 - f_{th}^{\nu_0}) \left(\frac{\nu}{\nu_0}\right)^{-\alpha_{nth}} \quad (1)$$

The first term on the right hand side of Eq. 1 describes the fractional thermal amount of the emission, the second one the synchrotron component. The used frequency dependences hold

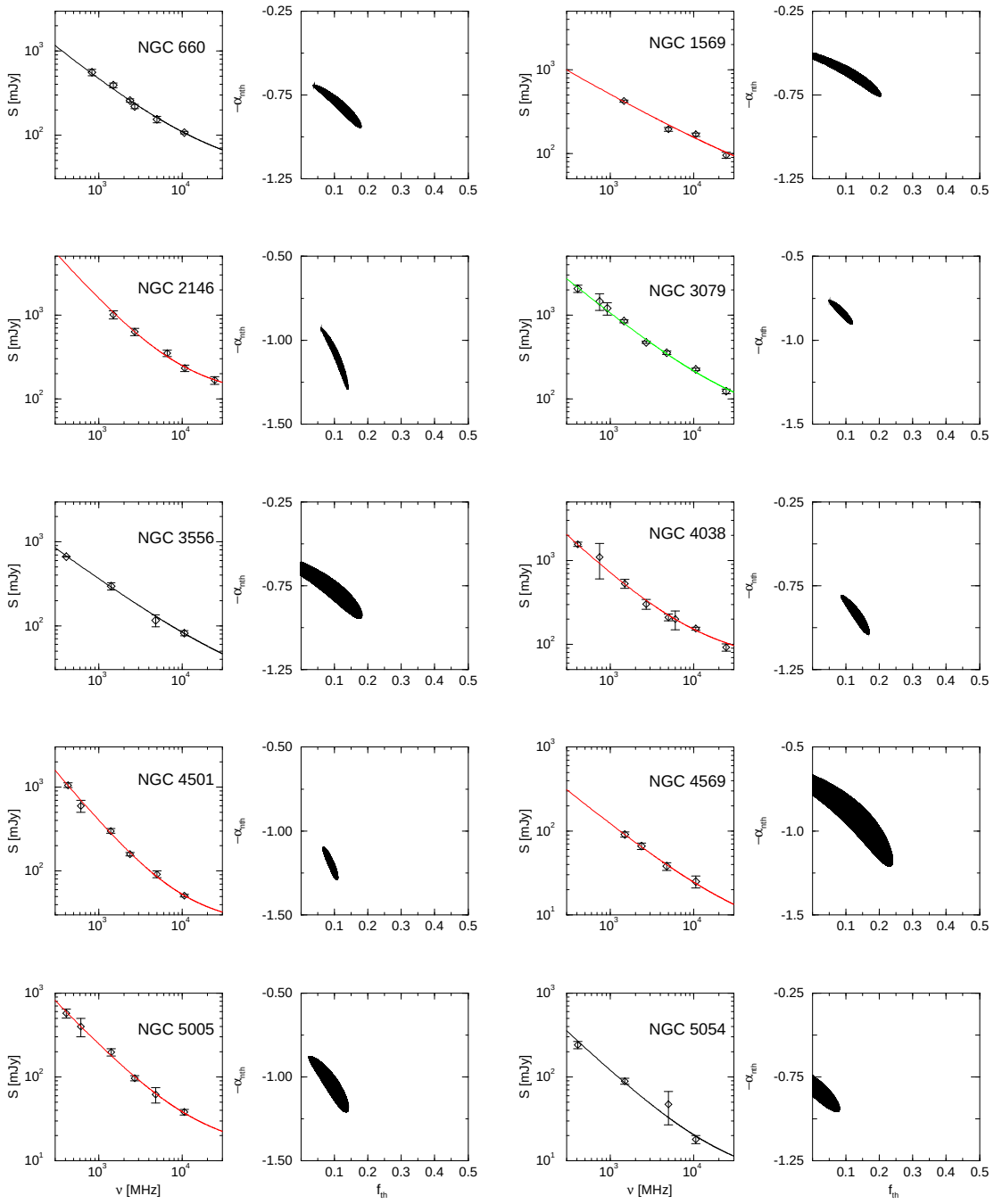

Fig. 1. Ten representative examples of galaxies with separated thermal and non-thermal radio emission. The left diagrams present the integrated radio spectra of the galaxies. The solid lines show the best fits to the spectra, with the parameters given in Table 1. The two-dimensional parameter space is plotted in the right diagrams. The black areas represents the 1-σ confidence regions

for the case of optically thin emission, an assumption which for the diffuse disk emission is valid. Furthermore, the model assumes that the synchrotron luminosity can be described by a single power-law. A more detailed discussion of Eq. 1 and its implications can be found in Duric et al. (1988). The assumption on the power-law nature of the non-thermal emission is valid if synchrotron and inverse Compton losses are not very strong and if galaxies do not show core emission. The curvature of a non-thermal radio spectrum with energy losses in the range of normal spiral galaxies is only slight (Condon 1992). Additionally, subtraction of thermal radio flux densities from the composite spectra yields in most cases a power-law or a concave residual spectrum indicating that energy losses have not affected the synchrotron spectra significantly. This will be discussed in more detail in Sect. 4. According to Paper I dominant radio emission from the nucleus is emitted only by galaxies

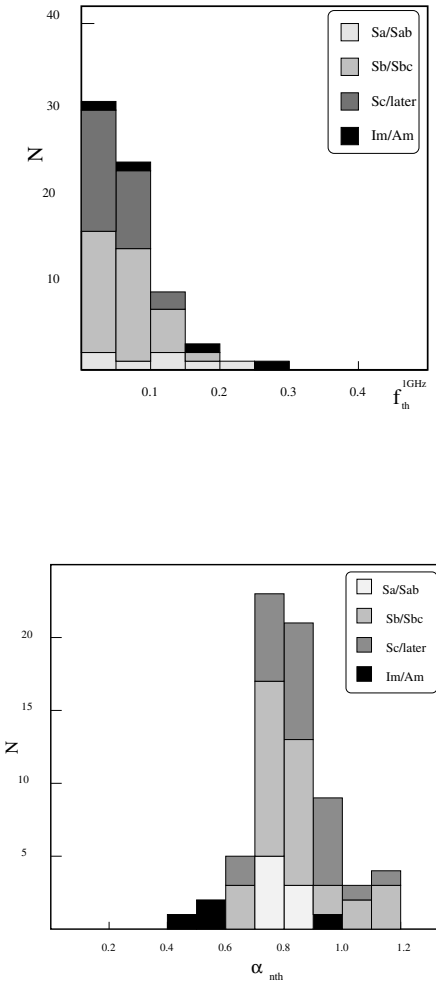

Fig. 2. The distribution of f_{th}^{1GHz} and α_{nth}. The upper diagram shows the distribution of f_{th}^{1GHz}, and the lower one the distribution of α_{nth}. The different morphological types in the galaxy sample are coded with different grey scales

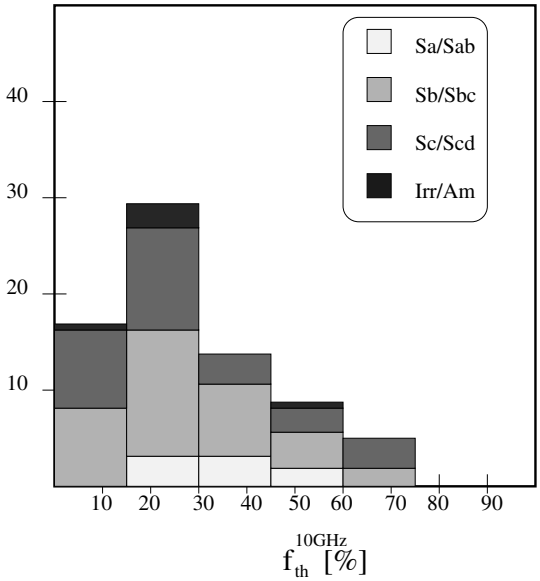

Fig. 3. The distribution of f_{th}^{10GHz}. The different grey scales represent the morphological types of the galaxies

of type Sa and Sab. The diffuse disk emission dominates the total emission for galaxies of later types. Therefore, we expect core emission to be important for less than 10% of our sample. The normalization frequency is $\nu_0 = 1$ GHz. Hence, there are two free parameters to fit: the thermal amount at 1 GHz f_{th}^{1GHz} and the non-thermal spectral index α_{nth}. The best-fit parameters were derived by minimizing the χ^2-function. Fig. 1 shows 10 representative examples for galaxies with separated thermal and non-thermal radio emission. Two diagrams are plotted for each galaxy. The left graph shows the mean integrated spectrum, and the solid line represents the fitted spectrum using the best-fit parameters given in the third and fourth column of Table 1. The black area in the right diagrams represents the 1-σ confidence range of the fitted parameters. The border of this area is given by pairs of α_{nth} and f_{th}^{1GHz}, where the χ^2-function has a value of $\chi^2 = \chi^2_{min} + 2.3$. χ^2_{min} is the χ^2-value of the best-fit parameter and the factor 2.3 is given by Lampton et al. (1976) for the 1-σ confidence range in case of a two-dimensional parameter space.

One can see that the size of this area is mainly determined by the number of data points. The more flux densites are known, the better the fit parameters are determined.

In Table 1 we have compiled the results of the separation for all 74 galaxies. The names of the galaxies and their morphological types are given in the first two columns. The best-fit parameters f_{th}^{1GHz} and α_{nth} are presented in Columns 3 and 4. The errors in f_{th}^{1GHz} and α_{nth} correspond to the 1-σ confidence interval at fixed α_{nth} and f_{th}^{1GHz}, respectively. In some cases the χ^2-fitting method yields the smallest χ^2-value for $f_{th}^{1GHz} = 0.0$. For such galaxies only upper limits to the thermal fraction are given. These correspond to the lower right border of the confidence region, i.e. the largest values of f_{th}^{1GHz} which fall in the 1-σ confidence area (e.g. NGC 5054 in Fig. 1). In these cases Column 4 contains the allowed range of α_{nth} from $f_{th}^{1GHz} = 0.0$ to the upper limit in f_{th}^{1GHz}. The fifth column shows the extrapolated thermal fraction at 10 GHz f_{th}^{10GHz}. The minimum χ^2-value is given in Column 6. The seventh column presents the number of degrees of freedom in the fit. The number of data points is reduced by one because of the normalization, and by two because of the two fit parameters. This gives $N_{df} = N_{data} - 3$. In the last column the references to the flux densities are listed.

3. Results of the separation

Fig. 2 shows the distribution of the derived quantities. The diagram at the top presents the distribution of f_{th}^{1GHz}, and the distribution of α_{nth} is plotted at the bottom. In case of galaxies with upper limits in f_{th}^{1GHz} the value of α_{nth} used is the mean of the range in α_{nth} given in Col. 4. The morphological types of the galaxies are coded with different grey scales. The mean values of the distributions with defined values are $\langle f_{th}^{1GHz} \rangle = 0.07 \pm 0.01$

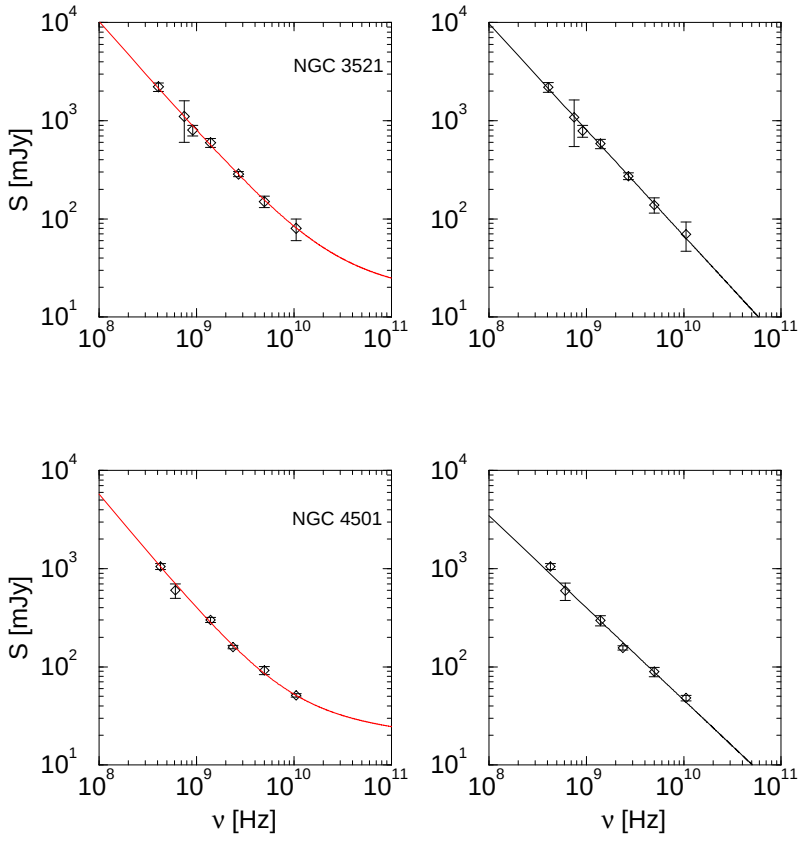

Fig. 4. Test of the separation by estimating the thermal radio flux using Hα data. The left diagrams show the integrated spectra for two representative examples. The line corresponds to the best-fit parameters of Table 1. The right graphs show the residual spectra after subtraction of the estimated thermal flux $S_{therm}^{H\alpha}$ from the Hα data

and $\langle\alpha_{nth}\rangle = 0.85 \pm 0.02$. The calculation of the mean values of the subsamples with defined f_{th}^{1GHz} and α_{nth} and of the subsamples with upper limits in the two quantities does not yield any significant differences in the statistical moments of the subsamples. In the further analysis, the upper limits were treated in the same way as the defined values. Hence, calculation of the mean values of f_{th}^{1GHz} and α_{nth} of all 74 galaxies yields $\langle f_{th}^{1GHz}\rangle = 0.08 \pm 0.01$ and $\langle\alpha_{nth}\rangle = 0.83 \pm 0.02$. The standard deviations of the distributions of f_{th}^{1GHz} and α_{nth} are $\sigma_{f_{th}} = 0.04$ and $\sigma_{\alpha_{nth}} = 0.13$, respectively. The extrapolation of the thermal fraction to 10 GHz yields a distribution which has a peak between 20 % and 30 % (Fig. 3). Only 15 % of the galaxies in our sample have a thermal fraction larger than $f_{th}^{10GHz} = 0.45$, so that the non-thermal emission dominates the radio emission of galaxies at 10 GHz. The mean value of the distribution of f_{th}^{10GHz} is $\langle f_{th}^{10GHz}\rangle = 0.30 \pm 0.05$. The distributions of f_{th}^{1GHz} and f_{th}^{10GHz} seem to be independent of morphological type.

On the other hand, the morphological type and the non-thermal spectral index are not completely uncoupled. The range of $0.55 \leq \alpha_{nth} \leq 0.75$ is mainly covered by irregulars and early-type spirals. Spiral galaxies of type Sc are found in the range of $\alpha_{nth} = 0.8 - 1.05$. A subdivision of the sample into three subsamples consisting of Sa/Sab, Sb/later and Irr/Am galaxies yields the following mean values for the non-thermal spectral indices:
$\langle\alpha_{nth}^{Sa/Sab}\rangle = 0.76\,,\ \sigma_{Sa/Sab} = 0.04$
$\langle\alpha_{nth}^{Sb/later}\rangle = 0.85\,,\ \sigma_{Sb/later} = 0.13$
$\langle\alpha_{nth}^{Irr/Am}\rangle = 0.74\,,\ \sigma_{Irr/Am} = 0.14.$

In case of early-type spirals the flat non-thermal spectral index may be influenced by emission from compact cores which may be present in them. In Paper I we have shown that the core emission dominates the total radio emission of spirals of type Sa and Sab. The emission of galactic nuclei often shows inverted radio spectra. This has been shown for e.g. NGC 4594 by de Bruyn et al. (1976). In case of core-dominated radio emission these inverted spectra can significantly flatten the integrated spectrum of a galaxy. The flat synchrotron spectra of some irregular and amorphous galaxies may indicate a high escape probability of cosmic ray electrons in these galaxies. According to Klein et al. (1991) the efficiency of particle confinement is lower in less massive galaxies. In these, the relativistic electrons can escape very easily from their host galaxies and have no time to undergo loss processes which would steepen the particle spectrum. Additionally, in actively star-forming galaxies the occurrence of winds may produce a flat synchrotron spectrum.

Eleven galaxies show very steep synchrotron spectra. ($\alpha_{nth} > 1.00$). This may indicate that synchrotron and inverse Compton losses are strongly affecting the relativistic electron population of these galaxies, which may happen if these galaxies efficiently confine the cosmic-ray particles.

Comparison with the study of radio spectral indices by Gioia et al. (1982) shows that the influence of the thermal emission flattens the radio spectrum of most of the galaxies. Our analysis agrees with the investigation of the radio spectra of

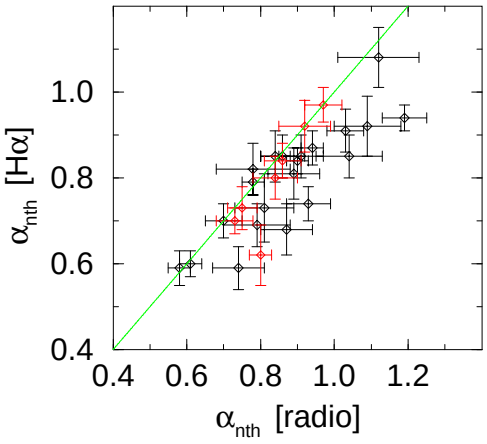

Fig. 5. Plot of non-thermal spectral indices $\alpha_{\rm nth}^{\rm H\alpha}$ obtained by an estimate of the thermal radio flux using the Hα data, versus the non-thermal spectral indices $\alpha_{\rm nth}$ obtained by fitting Eq. 1 to the integrated radio spectra. The solid line represents perfect agreement between the two quantities

13 galaxies by Klein (1988). The distribution of $\alpha_{\rm nth}$ derived by Klein (1988) yielded a mean non-thermal spectral index of $\langle\alpha_{\rm nth}\rangle = 0.88 \pm 0.08$. This is in good correspondence with Fig. 2, and in excellent agreement with our mean value. However, the larger number of galaxies and the high quality of the data of our analysis have strongly increased the statistical significance, which can be seen if one compares the dispersion in $\alpha_{\rm nth}$ in this work ($\sigma = 0.13$) with the dispersion derived by Klein (1988, $\sigma = 0.23$). Our separation of thermal and non-thermal radio emission disagrees with the results for 32 galaxies obtained by Duric et al. (1988). Their distribution of the spectral indices is in principle similar to Fig. 2, but Duric et al. found variations of the thermal fraction at 5 GHz from 0 % up to ∼90 %. These variations were not only found among different galaxy types, but also for galaxies of the same type. Furthermore, the results of Duric et al. (1988) suggest a coupling between the thermal fraction and non-thermal spectral index, in the sense that galaxies with a high thermal amount of emission exhibit steep non-thermal spectra. There exists no physical reason for this kind of a correlation, and it may be a selection effect produced by bad data. If one plots $f_{\rm th}^{\rm 1GHz}$ from Table 1 versus the corresponding $\alpha_{\rm nth}$, no correlation is found (correlation coefficient < 0.2). This shows that the statistical analysis of the data in our work is correct. In contrast to the findings of Duric et al. (1988), we can say that the constancy of $f_{\rm th}^{\rm 1GHz}$ and $\alpha_{\rm nth}$ indicates that the physical conditions in the interstellar medium do not vary strongly from galaxy to galaxy and that the non-thermal spectral index seems to be the same among all normal galaxies with a mean value of $\langle\alpha_{\rm nth}\rangle = 0.83$.

4. Are losses significant?

The separation of thermal and non-thermal emission is based on two assumptions about the physical conditions in galaxies. One is the assumption of optically thin emission, and the second is that the synchrotron emission of a galaxy can be described by a single power-law in the frequency range from ∼400 MHz up to 10 GHz. Especially the second assumption is critical, because of the effects of loss processes on high-energy electrons. Hence, it is possible that the high-frequency radio spectrum of a galaxy is affected by synchrotron losses. In this case, the above described method of the separation would underestimate the thermal amount, and the derived non-thermal spectral indices would be too flat.

In order to check this an independent estimate of the thermal radio flux density is necessary. It is possible to calculate the thermal radio flux from the emission in the Hα recombination line and an assumed thermal electron temperature T_e. The Hα emission in normal spiral galaxies is proportional to the free-free emission of thermal electrons in the HII regions. Using the equations of thermal free-free emission in an ionized gas one can compute the thermal radio flux density $S_{\rm th}$ from the Hα flux $S_{\rm H\alpha}$ in the following way (see e.g. Caplan & Deharveng 1986):

$$\left(\frac{S_{\rm th}}{\rm mJy}\right) = 2.238 \cdot 10^9 \cdot \left(\frac{S_{\rm H\alpha}}{\rm erg\,s^{-1}\,cm^{-2}}\right) \cdot \left(\frac{T_e}{\rm K}\right)^{0.42} \times \left\{\ln[\frac{0.04995}{(\nu/({\rm GHz})}] + 1.5 \cdot \ln\left(\frac{T_e}{\rm K}\right)\right\}. \quad (2)$$

Using Eq. 2 it is possible to calculate the thermal radio flux density at every frequency for a galaxy with a given Hα flux. Kennicutt & Kent (1983) carried out an Hα survey of normal galaxies. For 29 galaxies from Table 1 Hα fluxes were available from this survey. For these galaxies we calculated thermal radio fluxes $S_{\rm therm}^{\rm H\alpha}$ at those frequencies where radio flux densities are available, using Eq. 2. The assumed thermal electron temperature is 10^4 K. The thermal fluxes were subtracted from the flux densities at the corresponding frequencies in the integrated spectra. We fitted power-laws to the residual spectra in order to obtain the non-thermal spectral index $\alpha_{\rm nth}^{\rm H\alpha}$. The determination of $\alpha_{\rm nth}^{\rm H\alpha}$ and $\alpha_{\rm nth}$ is less sensitive to observational errors than the derived thermal flux densities because the non-thermal spectral indices do not depend on just one data point.

Fig. 4 shows two representative examples. In the case of complete elimination of the thermal component by the subtraction of $S_{\rm therm}^{\rm H\alpha}$ the residual spectrum will represent the pure synchrotron spectrum. The non-thermal spectral index from Table 1 and $\alpha_{\rm nth}^{\rm H\alpha}$ should be the same if loss processes have not significantly steepened the synchrotron spectrum. If energy losses are important the residual spectrum will show a steepening at shorter wavelengths, and $\alpha_{\rm nth}^{\rm H\alpha}$ should be larger than $\alpha_{\rm nth}$ from Table 1.

Fig. 5 shows $\alpha_{\rm nth}^{\rm H\alpha}$ plotted versus $\alpha_{\rm nth}$. There exists a clear correlation between the two quantities. This confirms the results of Table 1 and, in particular the wings of the distribution of $\alpha_{\rm nth}$ are not due to observational scatter. Hence, the values of $\alpha_{\rm nth}$ range indeed from ∼0.5 to ∼1.2. On the other hand, $\alpha_{\rm nth}^{\rm H\alpha}$ generally tends to be smaller than $\alpha_{\rm nth}$. This can be interpreted as an underestimate of the thermal emission using the Hα fluxes, owing to absorption of the Hα emission

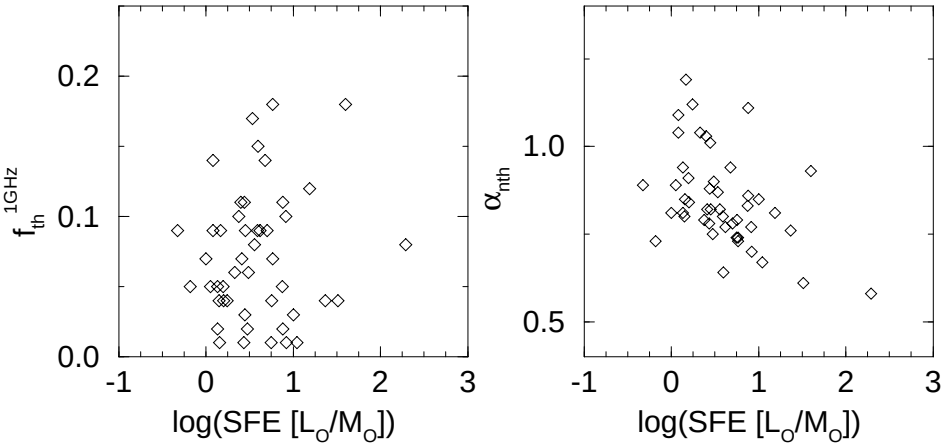

Fig. 6. The left diagram presents the plot of f_{th}^{1GHz} versus SFE, the right one shows α_{nth} plotted versus the SFE

by dust. On average, the difference between $\alpha_{nth}^{H\alpha}$ and α_{nth}^{radio} is $\Delta\alpha = 0.07$. The difference in the non-thermal spectral indices can be used to estimate the internal absorption. We assume a normal spiral galaxy with $\alpha_{nth}^{radio} = 0.83$ and $f_{th}^{1GHz} = 0.08$ evaluated from the radio spectrum. For the estimate of the Hα absorption we assume a total radio flux density $S_{tot}(\nu_1)$ at a frequency ν_1. With α_{nth}^{radio} and f_{th}^{1GHz} it is possible to calculate the total flux density $S_{tot}(\nu_2)$ at a second frequency ν_2, as well as thermal and non-thermal flux densities at both frequencies ($S_{th}^{radio}(\nu_1), S_{th}^{radio}(\nu_2), S_{nth}^{radio}(\nu_1)$ and $S_{nth}^{radio}(\nu_2)$). The smaller $\alpha_{nth}^{H\alpha}$ is produced by an underestimate of the thermal flux density $S_{th}^{H\alpha}$ using Hα data. This can be expressed by $S_{th}^{H\alpha} = k \times S_{th}^{radio}$ with $k < 1$. It is important to note that k is frequency independent. The ratio $S_{nth}^{H\alpha}(\nu_1)/S_{nth}^{H\alpha}(\nu_2)$ is given by $(\nu_1/\nu_2)^{-\alpha_{nth}^{H\alpha}}$. $S_{nth}^{H\alpha}$ can be replaced by $S_{tot} - S_{th}^{H\alpha}$ at both frequencies because the sum of thermal and non-thermal flux densities has to be the total flux density. Now we use $S_{th}^{H\alpha} = k \times S_{th}^{radio}$ and express $\alpha_{nth}^{H\alpha}$ as $\alpha_{nth}^{radio} - \Delta\alpha$. The ratio k between $S_{th}^{H\alpha}$ and S_{th}^{radio} is then given by:

$$k = \frac{S_{tot}(\nu_1) - S_{tot}(\nu_2)\left(\frac{\nu_1}{\nu_2}\right)^{-(\alpha_{nth}^{radio}-\Delta\alpha)}}{S_{th}^{radio}(\nu_1) - S_{th}^{radio}(\nu_2)\left(\frac{\nu_1}{\nu_2}\right)^{-(\alpha_{nth}^{radio}-\Delta\alpha)}} \quad (3)$$

Using k one can compute the internal Hα absorption $A_{H\alpha} = -2.5\log(k)$. As an example, for a *normal* spiral galaxy with $\alpha_{nth}^{radio} = 0.83$ and $f_{th}^{1GHz} = 0.08$ we assume a total radio flux density $S_{tot}(\nu_1 = 1\,GHz) = 100\,mJy$. The parameters of the radio continuum spectrum give then $S_{tot}(\nu_2 = 10\,GHz) = 20\,mJy$ and the thermal flux densities at 1 and 10 GHz are 8 and 6.4 mJy, respectively. This gives k = 0.5 and $A_{H\alpha} = 0.8^m$ using the average $\Delta\alpha = 0.07$. The choice of $S_{tot}(\nu_1)$ is arbitrary and the determination of k based solely on the parameters of the radio continuum spectrum and the difference between α_{nth}^{radio} and $\alpha_{nth}^{H\alpha}$.

Of course, this value is an approximation because the remaining curvature of the spectrum in case of an underestimated thermal flux was neglected. Nevertheless internal absorption of this magnitude is what one would expect for normal spiral galaxies.

5. Influence of star formation

A galaxy with strong star formation activity should have stronger thermal radio emission, due to the larger number of young, massive stars ionizing the interstellar hydrogen. Likewise, the larger number of massive stars increases the supernova rate which leads to a higher production of cosmic ray electrons. Therefore the synchrotron emission should also be increased. Hence, the thermal *fraction* of the radio emission is *not* directly coupled with the rate of star formation. According to Chi & Wolfendale (1990) the production and confinement of cosmic ray particles depends on the star formation rate. They expect steeper non-thermal spectra in case of enhanced star formation, owing to more efficient particle confinement.

The derived thermal fraction and the non-thermal spectral indices can be used to investigate the influence of star formation on the radio continuum emission of galaxies. The proportionality between the Hα and FIR-luminosity (e.g. Young et al. 1989) suggests the use of the FIR as a global measure for the star formation rate. Because a large galaxy will be more luminous in all frequency bands than a small one it is necessary to normalize the FIR luminosity. One way to do this is to use the mass of the molecular hydrogen. This bears the advantage that one deals with the quantity L_{FIR}/M_{H2}, the so-called star formation efficiency (SFE). For 47 galaxies M_{H2} was calculated using CO-line fluxes by Young et al. (1989) and by Solomon & Sage (1988). For both data sets the $N(H2)/I_{CO}$ conversion factor used was $2.8 \times 10^{20}\,cm^{-2}(K\,km\,s^{-1})^{-1}$ (Bloemen et al. 1986).

Fig. 6 shows plots of f_{th}^{1GHz} and α_{nth} versus the SFE. No correlation is evident between the thermal fraction f_{th}^{1GHz} and the SFE. This suggests that enhanced star formation will increase both, the thermal and non-thermal emission in the same proportions and on time scales which are small compared to the time scale of energy loss of the relativistic particles. However, the distribution of the points in the α_{nth} − SFE diagram exhibits the existence of an upper envelope, in such way that galaxies with a low SFE show steeper non-thermal spectra on average. If one divides the galaxy sample into a subsample with flat ($\alpha_{nth}^{flat} < 0.85$) and steep ($\alpha_{nth}^{steep} > 0.85$) synchrotron spectra and calculates the mean SFE for the different subsamples, then

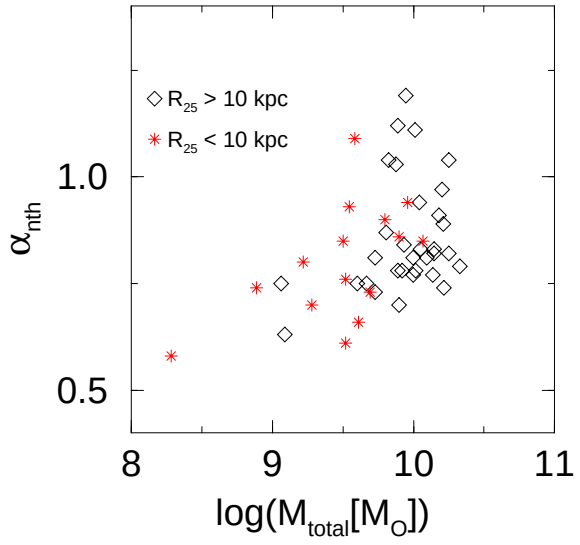

Fig. 7. The non-thermal spectral indices $\alpha_{\rm nth}$ plotted versus the total gas mass $M_{\rm total}$ of the atomic and molecular gas. The sample is divided into galaxies with $R_{25} < 10$ kpc (stars) and with $R_{25} > 10$ kpc (diamonds)

for $\alpha_{\rm nth}^{\rm flat}$ one obtains $\langle {\rm SFE} \rangle = (13 \pm 6) {\rm L}_\odot/{\rm M}_\odot$, and for $\alpha_{\rm nth}^{\rm steep}$ one gets $\langle {\rm SFE} \rangle = (5 \pm 2) {\rm L}_\odot/{\rm M}_\odot$. The non-thermal spectra of actively star forming galaxies appear to be closer to the injection spectra (e.g. Völk et al. 1988). With the assumption of equilibrium between the production of cosmic ray electrons and their energy losses this result implies that in galaxies with a high SFE one sees a younger relativistic electron population. In galaxies with a lower SFE the production rate of cosmic ray electrons is lower and, hence, the spectrum of the electrons is more strongly affected by losses.

Another point of interest is the efficiency of particle confinement. A galaxy that stores the cosmic ray particles very effectively should have a non-thermal spectral index ~ 1, assuming the usual injection spectral index. According to Chi & Wolfendale (1990) the particle confinement should be efficient in the largest and most FIR-luminous galaxies. However, a correlation between $\alpha_{\rm nth}$ and $L_{\rm FIR}$ can clearly be ruled out from our data. For the 47 galaxies with known H_2 masses, HI-masses were taken from Huchtmeier & Richter (1989), and the total gas mass $M_{\rm gas} = M_{\rm H2} + M_{\rm HI}$ of the interstellar gas computed. Fig. 7 shows the plot of $\alpha_{\rm nth}$ versus the $M_{\rm gas}$. The diamonds represent large galaxies ($R_{25} > 10$ kpc) and the stars small ones ($R_{25} < 10$ kpc). There exists a tendency from low-mass galaxies with flat spectra towards more massive galaxies with steep spectra. Also, smaller galaxies have flatter non-thermal spectra on average, indicating a less efficient particle confinement. This is consistent with the findings of Klein et al. (1991) who attribute the lack of non-thermal emission in Blue Compact Dwarf Galaxies to a high escape probability of the cosmic ray electrons in these low-mass systems. The fact that a significant number of galaxies seems to have a high escape probability for cosmic ray electrons sets also constraints on exisiting models of the radio-FIR correlation (e.g. Völk 1989, Lisenfeld et al. 1986). This subject is discussed in more detail by Niklas (1995) and Niklas & Beck (1996).

6. Summary

For a sample of 74 Shapley-Ames galaxies thermal and non-thermal radio emission was separated. The mean value of the non-thermal spectral index is $\langle \alpha_{\rm nth} \rangle = 0.83 \pm 0.02$. On average one third of the radio continuum emission at 10 GHz can be attributed to thermal free-free emission. An independent estimate of the thermal amount using Hα data yields that energy lossses of the cosmic ray electrons do not significantly steepen the radio continuum spectrum in the GHz-frequency regime. The mean extinction of the Hα emission by dust was determined to be $A_{\rm H\alpha} = 0.8^{\rm m}$.

Large and massive galaxies with low SFE tend to have flatter non-thermal spectral indices than low mass-galaxies with high star formation actvitity. The presented correlations are not very tight, but this may be attributed to the uncertainties in the calculation of the mass of the molecular hydrogen. Nevertheless, we found that the star formation efficiency as well as mass and size of a galaxy affects the population of the synchrotron emitting electrons.

Acknowledgements. We thank the anonymous referee for a number of comments making the presentation of the paper more clear. The authors are grateful to Dr. J. Braine for helpful discussion and various useful suggestions in the course of this work. SN was supported by the Max-Planck-Gesellschaft during his PhD.

References

Baars, J.W.M., Genzel, R., Pauliny-Toth, I.I.K., Witzel, A. 1977, A&A 61, 99
Beck, R., Klein, U., Krause, M. 1985, A&A 152, 23
Beck, R., Carilli, C.L., Holdaway, M.A., Klein, U. 1994, A&A 292, 409
Bloemen, J.B.G.M., Strong, A., Blitz, L., Cohen, R.S., Dame, R.S. et al. 1986, A&A 154, 25
Bogdan, T.J., Völk, H.J. 1983, A&A 122, 129
Branson, N. 1967, MNRAS 135, 149
Caplan, J., Deharveng L. 1986, A&A 155, 297
Chi, X., Wolfendale, A.W. 1990, MNRAS 245, 101
Condon, J.J. 1983, ApJS 53, 459
Condon, J.J. 1987, ApJS 65, 485
Condon, J.J. 1992, ARAA 30, 575
Condon, J.J., Anderson, M.L., Helou, G. 1991, ApJ 376, 95
Cox, M.J., Eales, S.A., Alexander, P., Fitt, A.J. 1988, MNRAS 235, 1227
de Bruyn, A.G., Crane, P. C., Price, R.M., Carlson, J.B. 1976, A&A 46, 243
Dressel, L.L., Condon, J.J. 1978, ApJS 36, 53
Dumke, M., Krause, M., Wielebinski, R., Klein, U. 1995, A&A 302, 691
Duric, N., Borneuf, E., Gregory, P.C. 1988, AJ 96, 81
Ehle, M., Beck, R. 1993, A&A 273, 45
Garcia-Baretto, J.A., Carillo, R., Klein, U., Dahlem, M. 1993, Rev. Mex. Astron. Astrofis. 25, 31
Gioia, I.M., Fabbiano, G. 1987, ApJS 63, 771

Gioia, I.M., Gregorini, L. 1980, A&AS 41, 329
Gioia, I.M., Gregorini, L., Klein, U. 1982, A&A 116, 164
Gräve, R., Klein, U., Wielebinski, R. 1981, A&A 95, 391
Gräve, R., Klein, U., Wielebinski, R. 1990, A&A 238, 39
Harnett, J.I. 1982, Aust. J. Phys. 35, 321
Haynes, R.F., Sramek, R. 1975, AJ 80, 673
Haynes, R.F., Huchtmeier, W.K., Siegman, B.C., Wright, A.E. 1975, A Compendium of Radio Measurements of Bright Galaxies, CSIRO Division of Radiophysics, Melbourne
Huchtmeier, W.K. 1975, A&A 44, 101
Huchtmeier, W.K., Richter, O.-G. 1989, A General Catalog of HI Observations of Galaxies (New York, Springer Verlag)
Hummel, E. 1980, A&AS 41, 151
Hummel, E., Beck, R. 1995, A&A 305, 691
Hummel, E., Beck, R., Dettmar, R.-J. 1991a, A&AS 87, 309
Hummel, E., Dahlem, M., van der Hulst, J.M., Sukumar, S. 1991b, A&A,246, 10
Israel, F.P., Mahoney, M.J. 1990, ApJ 352, 30
Israel, F.P., van der Hulst, J.M. 1983, AJ 88, 1736
Kazès, A.M., Nguyen-Quang-Rieu 1970, Astr. Let. 6, 193
Kellermann, K.I., Pauliny-Toth, I.I., Williams, P.J. 1969, ApJ 157, 1
Kennicutt, R.C., Kent, S.M. 1983, AJ 88, 1094
Klein, U. 1988, Habilitation Thesis, Univ. Bonn
Klein, U., Emerson, D.T. 1982, A&A 94, 29
Klein, U., Gräve, R. 1986, A&A 161, 155
Klein, U., Urbanik, M., Beck, R., Wielebinski, R. 1983, A&A 127, 177
Klein, U., Wielebinski, R., Morsi, H.W. 1988, A&A 190, 41
Klein, U., Weiland, H., Brinks, E. 1991, A&A 246, 323
Lampton, M., Margon, B., Bowyer, S. 1976, ApJ 208, 177
Lequeux, J. 1971, A&A 15, 30
Lerche, I., Schlickeiser, R. 1982, A&A 107, 148
Lisenfeld, U. Völk, H.J., Xu, C. 1996, A&A 306, 677
Neininger, N. 1992, A&A 263, 30
Neininger, N., Klein, U., Beck, R., Wielebinski, R. 1991, Nat 352, 781
Niklas, S. 1995, PhD Thesis, Univ. Bonn
Niklas, S., Beck, R. 1996, A&A, subm.
Niklas, S., Klein, U., Braine, J., Wielebinski, R. 1995, A&AS 114, 21
Pacholczyk, A.G. 1970, Radio Astrophysics, W.H. Freeman and Company, San Francisco
Reakes, M. 1980, MNRAS 192, 297
Segalovitz, A. 1977, A&A 55, 203
Solomon, P.M., Sage, L.J. 1988, ApJ 334, 613
Sramek, R. 1975, AJ 80, 771
Sukumar, S., Velusamy, T., Klein, U. 1988, MNRAS 231, 765
Sulentic, J.W. 1976, ApJS, 32, 171
Urbanik, M., Gräve, R., Klein, U. 1985, A&A 152, 291
Urbanik, M., Gräve, R., Klein, U. 1986, A&A 166, 107
von Kap-herr, A., Jones, B.B., Wielebinski, R. 1975, A&A 41, 115
Völk, H.J. 1989, A&A 218, 67
Völk, H.J., Zank, L.A., Zank, G.P. 1988, A&A 198, 274
Whiteoak, J.B. 1970, Astr. Let. 5, 29
Wunderlich, E., Klein, U., Wielebinski, R. 1987, A&AS 69, 487
Young, J., Xie, S., Kenney, J., Wice, W.L. 1989, ApJS 70, 699

This article was processed by the author using Springer-Verlag LaTeX A&A style file *L-AA* version 3.